







**Table 1.** The interpolation kernels  $\mathbf{U}$  used in the present study, as derived from continuum elastic theory (see text)

Spline type	Deformation term
TPS	$\mathbf{U}( \mathbf{p} ) =  \mathbf{p} \mathbf{I}$
EBS Kernel 1	$\mathbf{U}( \mathbf{p} ) = [(11 - 12\nu) \mathbf{p} ^2\mathbf{I} - 3\mathbf{p}\mathbf{p}^T] \mathbf{p} $
EBS Kernel 2	$\mathbf{U}( \mathbf{p} ) = (7 - 8\nu) \mathbf{p} \mathbf{I} - \frac{1}{ \mathbf{p} }\mathbf{p}\mathbf{p}^T$

$\mathbf{I}$  - the  $3 \times 3$  identity matrix,  $\nu$  - EBS elasticity coefficient

displacement compared to distant vectors. Shepard (1968) formulated the smooth (continuous and once differentiable) function

$$\mathbf{f}(\mathbf{p}) = \frac{\sum_{i=1}^N \text{weight}(\mathbf{p}, \mathbf{w}_i) \cdot (\mathbf{w}_i^{\text{em}} - \mathbf{w}_i^{\text{calc}})}{\sum_{i=1}^N \text{weight}(\mathbf{p}, \mathbf{w}_i)}, \quad (4)$$

where  $\text{weight}(\mathbf{p}, \mathbf{w}_i^{\text{calc}})$  is the weight of the  $i$ -th feature vector. Similar to spline interpolation, IDW ensures the exact fit of the feature vectors (see Equation 2). Usually the weighting function  $\text{weight}(\mathbf{p}, \mathbf{w}_i^{\text{calc}})$  is a monotonously decreasing function of the distance  $|\mathbf{p} - \mathbf{w}_i^{\text{calc}}|$ . Shepard (1968) proposed a global weighting scheme based on a negative power function:

$$\text{weight}(\mathbf{p}, \mathbf{w}_i^{\text{calc}}) = |\mathbf{p} - \mathbf{w}_i^{\text{calc}}|^{-c}, \quad (5)$$

while Franke and Nielson (1980) introduced a local IDW interpolation defined as

$$\text{weight}(\mathbf{p}, \mathbf{w}_i^{\text{calc}}) = \left[ \frac{\max(0, R - |\mathbf{p} - \mathbf{w}_i^{\text{calc}}|)}{R \cdot (|\mathbf{p} - \mathbf{w}_i^{\text{calc}}|)} \right]^c, \quad (6)$$

where  $c$  and  $R$  are constant parameters. The weighting exponent  $c$  influences the smoothness of the interpolator, and is required to exceed the value of 1 to ensure the differentiability of the function  $\mathbf{f}$ . Large exponents  $c > 8$  render the closest feature vector dominant, thereby decreasing the importance of the others. The influence radius,  $R$ , is determined as the distance accommodating a constant number of feature points defined by the user.

**2.3.3 Stereochemical idealization** One of the concerns in any refinement method is the stereochemical quality of resulting models. The original constrained MD approach automatically optimized and relaxed bonded and non-bonded interactions during the flexing based on a physical force field. The much simpler interpolation is of course lacking such stereochemical optimization. One could apply MD to such a model in a post-processing step but this would defeat the purpose of the intended simplification. As a compromise between usability by non-experts and the stereochemical quality we tested an optional idealization with the crystallographic refinement tool RefMac (Murshudov *et al.*, 1997) that regularizes abnormal bonds and angles. RefMac has the advantage that it is robust in the case of missing atoms and unknown substrates, whereas MD is very sensitive to such modeling inaccuracies. The tool is freely available to academic users but requires some extra work to be set up, therefore we have evaluated the performance of interpolation both in the presence and absence of the RefMac idealization, to test whether the improvements in stereochemistry justify the added effort.

### 3 RESULTS

We have tested the interpolation methods on three displacement data sets generated in our recent work: the bacterial RNA polymerase (RNAP), the chaperonin GroEL and the motor domain S1 of myosin. These systems exhibit large conformational changes during their

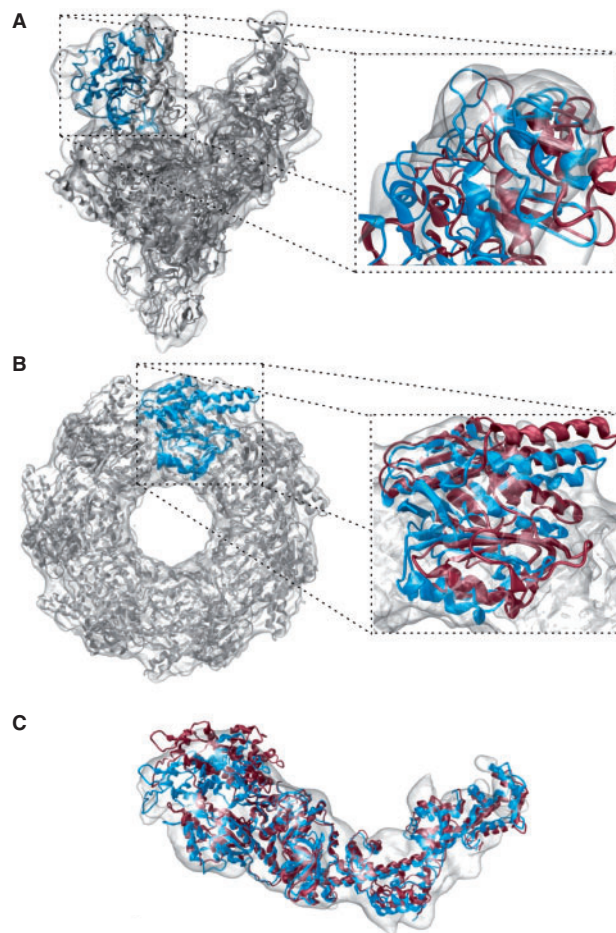


**Fig. 2.** Comparison of the interpolation based flexible fitting relative to the rigid body docking. Atomic models of volumetric map are built by rigid body registration (red ribbons), and refined by spatial IDW interpolation (blue, gray ribbons). (A) RNAP; left: side view; right: clamp domain. (B) GroEL; left: top view; right: one monomer. (C) Myosin.

functional cycles. In each case, the experimental cryo-EM map deviates significantly from the atomic structures (Fig. 2), requiring a flexible fit to account for the conformational change. The fitting was validated in discussion with our collaborators to ensure a sound interpretation.

In the following tests, we assess the quality of interpolation methods by comparing the resulting fitted structures with those derived by the well established constrained MD approach (Wriggers *et al.*, 2004) using identical input data (atomic structures and feature-vectors). The docking accuracy is assessed by the root mean square deviation (RMSD) of the  $C_\alpha$  as shown in Figure 3. Detailed numerical values and timings of all results are given in Supplementary Table 1.

In addition, one can study the structural differences in more detail through the native overlap (NO) well known in the homology modeling field (Fig. 4). The NO quantifies the percentage of atoms with spatial shift below a threshold value. For instance, NO3 represents the percentage of atoms deviating less than  $3 \text{ \AA}$  between the model generated by interpolation and the one obtained by constrained MD.

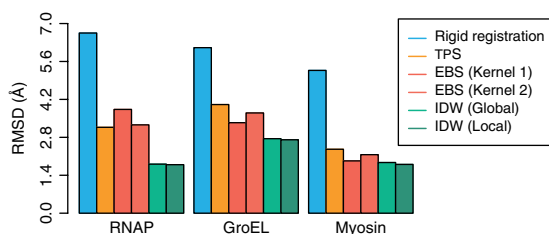


**Fig. 3.** RMSD from models generated with constrained MD.

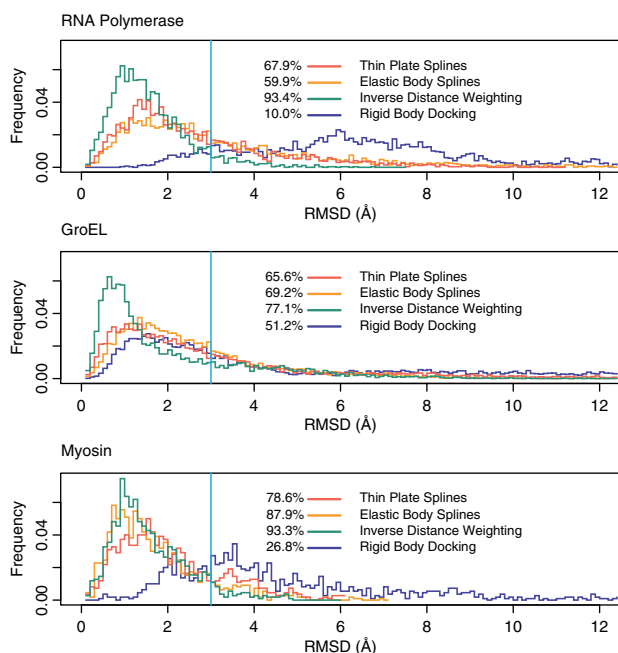


**Fig. 4.** Histogram of observed  $C_{\alpha}$  RMSDs. Shown are observed frequencies as a function of the deviation between the models and constrained MD. The percentage of atoms with deviations below  $3\text{Å}$  (NO3) is shown at the left hand side of the legend. Due to similarity with kernel 2, only kernel 1 of the EBS is shown. For the IDW the local weighting scheme with  $c=4$  and  $R$  holding nine feature vectors was used. Also shown for comparison are the deviations for the rigid body fit.

An even more detailed view is provided by the histogram of root mean square (RMS) positional deviations. The similarity can be qualitatively assessed by the width of the histogram around small values, i.e. a narrow histogram implies that a large number of atoms have small shifts between the two models while only few atoms have significantly larger ones. For all interpolation methods, the histograms of the RMS positional deviations are compared to those of the rigid body model in Figure 4.

For the cases we studied here there are no known atomic conformations of the target. However, we offer the cross-correlation with the EM map as an ‘absolute’ criterion of accuracy.

### 3.1 Opening of RNAP

We originally developed our flexible fitting techniques in collaboration with Seth Darst, whose laboratory determined the structure of *Escherichia coli* core RNAP by cryo-EM and image

processing of helical crystals to a resolution of  $15\text{Å}$ . The high sequence conservation between the core RNAP subunits enabled us to interpret the *E. coli* structure in relation to the high-resolution X-ray structure of *Thermus aquaticus* core RNAP. A very large conformational change of the *T. aquaticus* RNAP X-ray structure, corresponding to opening of the main DNA/RNA channel by nearly  $25\text{Å}$ , was required to fit the *E. coli* map (Fig. 2A). This finding reveals, at least partially, the range of conformational flexibility of the RNAP, which is likely to have functional implications for the initiation of transcription, where the DNA template must be loaded into the channel (Borukhov and Lee, 2005). Darst *et al.* (2002) flexed the crystal structure of *T. aquaticus* RNAP into the *E. coli*  $15\text{Å}$ -resolution cryo-EM map by constrained MD on 15 feature vectors. This simulation induced a  $6.65\text{Å}$  RMSD in the atomic structure. In a later study, the MD flexing technology enabled the location of the transcription elongation factor GreB bound to bacterial RNAP (Opalka *et al.*, 2003).

Based on the displacements measured at 15 feature vector positions (Darst *et al.*, 2002) we have reproduced the earlier MD flexing with the new interpolation methods. With respect to the MD structure, the models flexed by spline interpolations deviate by  $3.17\text{Å}$  for TPS and  $3.26\text{--}3.83\text{Å}$  for EBS (Fig. 3). In contrast, the IDW-refined model deviates by only  $1.79\text{Å}$  using the local scheme with  $c=4$  and cut-off distance  $R$  set to include the nine closest feature vectors (Equation 6). A similar deviation was also observed for the model generated by global IDW interpolation for  $c=8$  (Fig. 3). Relative to the initial rigid body docked conformation, the interpolation methods considerably increase the NO3 with the MD structure, from the initial value of 10.0% to at least 59.9%. Moreover, the IDW averaging exhibited the highest NO3 among the interpolation methods (93.4% versus 67.9% for TPS, 59.9% for EBS), and the sharpest histogram of RMS positional deviations (Fig. 4).

### 3.2 Flexibility of GroEL apical domains

Another system in the benchmark, the bacterial chaperonin GroEL, plays an important role in the native folding of proteins (Fenton and Horwich, 2003). The binding of ATP and of the co-chaperonin GroES initiate a series of allosteric rearrangements in GroEL’s structure that allow non-native proteins to interact with the chaperonin’s central channel, facilitating their refolding into the native state (Ranson *et al.*, 2001). Despite the large number of solved structures showing GroEL alone or in complex, the mechanism of protein folding by the chaperonin remains unclear.

To shed light on the structure–function relationship, one can investigate functionally relevant conformations. In one such experiment, the mutant Asp155→Ala was imaged by cryo-EM at  $14\text{Å}$  resolution (S.G. Wolf, D. Rivenzon-Segal, W. Wriggers and A. Horovitz, submitted for publication). The significant conformational changes observed in the apical domains of the mutant GroEL motivated us to consider this system in the benchmarking of the interpolation methods. The rigid body docking of the complex identified the locations of the 14 monomers (PDB entry 1xck; Berman *et al.* 2000) in the 3D map, and emphasized the conformational differences in the datasets (Fig. 2B). The docked crystal structure was refined against the cryo-EM map by MD simulations constrained to 112 feature vectors, or eight vectors per monomer. This refinement procedure induced a large ( $6.11\text{Å}$

RMSD) conformational change in the GroEL structure, mainly in the apical domains that exhibit considerable variability. Here, we used the 112 displacements from the MD study for a performance test of the interpolation methods.

Considering the large size of this system, the interpolated models agree reasonably well with the MD result. We achieved RMS deviations of 4.01 Å for TPS and 3.34–3.70 Å for EBS (Fig. 3). However, the IDW-based model deviates only 2.75 Å, in the case of global IDW ( $c = 8$ ), and 2.71 Å in the case of local IDW ( $c = 4$ ,  $R$  set to include the nine closest feature vectors). Furthermore, similar to the RNAP case, the NO3 value of the IDW interpolation is superior to that of the splines (77.1% versus 65.6% and 69.2%), while the histogram of RMS positional deviations is also the sharpest (Fig. 4).

### 3.3 The actin-binding cleft closure of myosin S1

Myosin, the third system in the benchmark, is a molecular motor involved in both intra-cellular motility and muscle contraction (Geeves and Holmes, 1999; Rayment *et al.*, 1993). Here, we focus on the conformational differences induced by binding of S1 to the actin filament. A cryo-EM reconstruction of the actomyosin complex at 14 Å resolution was recently determined by our collaborator Rasmus Schröder (Holmes *et al.*, 2003). A fitted F-actin model (Holmes *et al.*, 2003) allowed us to create a mask for segmenting out a single myosin S1 unit (W. Wriggers and R.R. Schröder, unpublished data). This single myosin S1 map can then be compared to the atomic structure. We first attempted rigid body fitting of the atomic model, taken from the supplementary structure ‘motor\_domain.pdb’ published by Holmes *et al.* (2003). Rigid body docking was not satisfactory with respect to the position of the upper 50 K domain and the lever arm (Rayment *et al.*, 1993) even when performed independently for each structural subunit. Therefore we subjected the predicted atomic model to flexible docking (Fig. 2C) to characterize the observed changes.

The atomic model is allowed to move according to displacements tracked by 10 feature vectors. Our conservative choice of 10 feature vectors (corresponding to a spatial resolution of 26 Å in our coarse model) was sufficient to track shape changes while avoiding an over-fitting of the cryo-EM data. The MD refinement generated an overall 5.27 Å RMSD conformational change. The RMSD of the interpolated models relative to MD ranges from 2.36 Å for TPS, 1.93–2.16 Å for EBS, to 1.80–1.87 Å for the IDW interpolation (Fig. 3). The NO3 increased significantly from 26.8% for the initial structure to values ranging between 78.6–93.3% for the interpolation-based models, with the highest values achieved again by IDW (Fig. 4).

## 4 DISCUSSION

In this study, we evaluated three well-known interpolation methods for the flexible fitting of atomic structures into low-resolution data. We introduced interpolation as an efficient and easy-to-use alternative to constrained MD, with the goal of making the flexible fitting techniques available to non-expert users. Sampling the conformational variability by feature vectors limits the effect of experimental noise while avoiding over-fitting of low-resolution data. We expect our work to be generally useful for all applications where sparsely sampled displacements from coarse models are extended to a higher level of detail.

Visual inspection of the fit (Fig. 2) demonstrates a significant improvement of the best performing IDW fitting relative to rigid body docking. The two IDW methods described here rely at most on two parameters for which we provide empirical values based on exhaustive exploration of the parameter space. Our tests showed that the local IDW with a weighting exponent  $c$  set from 3–4 and a radius of influence  $R$  holding 50–90% of the feature vectors gives optimal results, similar to the global scheme with  $c$  set from 7–9. The type of IDW scheme and the exact values within the given ranges of  $c$  (or  $R$ ) are not critical (Supplementary Table 2), and in all cases the results were better or comparable to those of the other interpolation methods. If the number of parameters is a concern, global IDW has only one parameter which can remain fixed at  $c = 8$  for all practical purposes.

Our validation strategy was motivated by our goal to emulate the expensive MD results as well as possible with user friendly interpolation. We focused on measurable deviations between MD and interpolation at the carbon alpha level, excluding all possible sources of error except those due to interpolation. There are additional system dependent uncertainties in flexible fitting, for example due to experimental noise in the cryo-EM maps, or as mentioned above, due to the inherent ambiguity of placing many thousands of atoms into a low-resolution dataset (Wriggers, 2004). These sources of error are outside the scope of the current article and discussed in more detail elsewhere (Baker and Johnson, 1996; Stowell *et al.*, 1998; Wriggers and Chacón, 2001). However, we acknowledge that any flexible refinement will be judged by the accuracy of the fit to the experimental data. Therefore, we computed also the overlap between the experimental cryo-EM map and the flexed atomic models (low-pass filtered to experimental resolution) by the standard cross-correlation coefficient (Wriggers and Chacón, 2001). As expected, the flexed correlation values are all higher (Supplementary Table 1) than those of the initial structure. We also confirmed that the interpolated models exhibit very similar cross-correlations compared to the MD fit (Supplementary Table 1). The cross-correlation coefficients are nearly identical for interpolation methods and constrained MD because correlation (at low resolution) is not sufficient to differentiate between alternative models (Wriggers, 2004). However, we found that the IDW interpolation deviates least from constrained MD, showing minimal RMSD, narrowest histogram and maximal NO3 (Figs. 3 and 4) among the tested methods.

To regularize the bonds and angles disturbed by interpolation we carried out an additional idealization with the crystallization refinement tool RefMac (Murshudov *et al.*, 1997). Our tests found very minor improvements in RMSD values that are negligible at the  $C_{\alpha}$  level (Supplementary Table 2). This is to be expected as RefMac mainly regularizes the bonded interactions and the  $C_{\alpha}$  representation is itself a coarse model. Any post-processing of the warped structures with tools like RefMac will be beneficial, especially if all atoms of the system are considered. But our results suggest that for carbon alpha level accuracy it is not necessary to carry out an additional stereochemical refinement step.

In summary, the IDW interpolation methods described in this article are efficient alternatives to the constrained MD, enabling non-expert users to perform multiscale modeling tasks within seconds of compute time (Supplementary Table 1). These methods will be made available both as a command line tool ‘qplasty’

in the Situs package (<http://situs.biomachina.org>) and as part of the molecular visualization and modeling application Sculptor (<http://sculptor.biomachina.org>).

## ACKNOWLEDGEMENTS

We thank Rasmus R. Schröder, Kenneth C. Holmes, Dalia Segal, Sharon Wolf and Amnon Horovitz for discussions, and Michael E. Brandt and Jochen Heyd for critical reading of the article.

*Funding:* NIH (R01GM62968 to W.W.); Human Frontier Science Program (RGP0026/2003 to W.W.); Startup funds of the University of Texas Health Science Center at Houston (to S.B.) Supported by a training fellowship from the W. M. Keck foundation to the Gulf Coast Consortia through the Keck Center for Interdisciplinary Bioscience Training (M.R.).

*Conflict of Interest:* none declared.

## REFERENCES

- Alberts, B. (1998) The cell as a collection of protein machines: preparing the next generation of molecular biologists. *Cell*, **92**, 291–294.
- Baker, T.S. and Johnson, J.E. (1996) Low resolution meets high: towards a resolution continuum from cells to atoms. *Curr. Opin. Struct. Biol.*, **6**, 585–594.
- Baumeister, W. and Steven, A.C. (2000) Macromolecular electron microscopy in the era of structural genomics. *Trends Biochem. Sci.*, **25**, 624–631.
- Berman, F.C. et al. (2000) The protein data bank. *Nucleic Acids Res.*, **28**, 235–242.
- Birmanns, S. and Wriggers, W. (2007) Multi-resolution anchor-point registration of biomolecular assemblies and their components. *J. Struct. Biol.*, **157**, 271–280.
- Bookstein, F.L. (1989) Principal warps: thin-plate splines and the decomposition of deformations. *IEEE Trans. Pattern Anal. Mach. Intell.*, **11**, 567–585.
- Borukhov, S. and Lee, J. (2005) RNA polymerase structure and function at lac operon. *C. R. Biol.*, **328**, 576–587.
- Chapman, M.S. (1995) Restrained real-space macromolecular atomic refinement using a new resolution-dependent electron-density function. *Acta Cryst. A*, **51**, 69–80.
- Chen, J. et al. (2003) Low-resolution structure refinement in electron microscopy. *J. Struct. Biol.*, **144**, 144–151.
- Chou, P.C. and Pagano, N.J. (1967) *Elasticity: Tensor, Dyadic and Engineering Approaches*. Van Nostrand, Princeton, NJ.
- Darst, S. et al. (2002) Conformational flexibility of bacterial RNA polymerase. *Proc. Natl. Acad. Sci. USA*, **99**, 4296–4301.
- Davis, M.H. et al. (1997) A physics-based coordinate transformation for 3-D image matching. *IEEE Trans. Med. Imaging*, **16**, 317–328.
- Fenton, W.A. and Horwich, A.L. (2003) Chaperonin-mediated protein folding: fate of substrate polypeptide. *Quart. Rev. Biophys.*, **36**, 229–256.
- Frank, J. (2002) Single-particle imaging of macromolecules by cryo-electron microscopy. *Ann. Rev. Biophys. Biomol. Struct.*, **31**, 303–319.
- Frank, R. and Nielson, G. (1980) Smooth interpolation of large sets of scattered data. *Int. J. Numer. Methods Eng.*, **15**, 1691–1704.
- Gao, H. and Frank, J. (2005) Molding atomic structures into intermediate-resolution cryo-EM density maps of ribosomal complexes using real-space refinement. *Structure*, **13**, 401–406.
- Geeves, M.A. and Holmes, K.C. (1999) Structural mechanism of muscle contraction. *Ann. Rev. Biochem.*, **68**, 687–728.
- Gerstein, M. et al. (1994) Structural mechanisms for domain movements in proteins. *Biochemistry*, **33**, 6739–6749.
- Gordon, W.J. and Wixom, J.A. (1978) Shepard's method of 'metric interpolation' to bivariate and multivariate interpolation. *Math. Comput.*, **32**, 253–264.
- Harder, R.L. and Desmarais, R.N. (1972) Interpolation using surface splines. *J. Aircr.*, **9**, 189–191.
- Holmes, K.C. et al. (2003) Electron cryo-microscopy shows how strong binding of myosin to actin releases nucleotide. *Nature*, **425**, 423–427.
- Jolley, C.C. et al. (2008) Fitting low-resolution cryo-EM maps of proteins using constrained geometric simulations. *Biophys. J.*, **94**, 1613–1621.
- Murshudov, G.N. et al. (1997) Refinement of macromolecular structures by the maximum-likelihood method. *Acta Crystallogr. D.*, **53**, 240–255.
- Niemann, H.H. et al. (2008) X-ray and neutron small-angle scattering analysis of the complex formed by the Met receptor and the *Listeria monocytogenes* invasion protein InlB. *J. Mol. Biol.*, **377**, 489–500.
- Opalka, N. et al. (2003) Structure and function of the transcription elongation factor GreB bound to bacterial RNA polymerase. *Cell*, **114**, 335–345.
- Orzechowski, M. et al. (2008) Molecular Dynamics Flexible Fitting (MDFF) – A Novel Method for Cryo-EM Maps Refinement. *Biophys. J.*, **94**, 1753 [Abstract].
- Rai, N. et al. (2005) SOMO (SOLUTIONModeler): Differences between X-ray and NMR-derived bead models suggest a role for side chain flexibility in protein hydrodynamics. *Structure*, **13**, 723–734.
- Ranson, N.A. et al. (2001) ATP-bound states of GroEL captured by cryo-electron microscopy. *Cell*, **107**, 869–879.
- Rayment, I. et al. (1993) Three-dimensional structure of myosin subfragment-1: a molecular motor. *Science*, **261**, 50–58.
- Shepard, D. (1968) A two-dimensional interpolation function for irregularly-spaced data. In *Proceedings of the 1968 23rd ACM National Conference*. ACM, NY, pp. 517–524.
- Stowell, M.H.B. et al. (1998) Macromolecular structure determination by electron microscopy: new advances and recent results. *Curr. Opin. Struct. Biol.*, **8**, 595–600.
- Tama, F. et al. (2004) Flexible multi-scale fitting of atomic structures into low-resolution electron density maps with elastic network normal mode analysis. *J. Mol. Biol.*, **337**, 985–999.
- Topf, M. and Šali, A. (2005) Combining electron microscopy and comparative protein structure modeling. *Curr. Opin. Struct. Biol.*, **15**, 578–585.
- Trabuco, L.G. et al. (2008) Flexible fitting of atomic structures into electron microscopy maps using molecular dynamics. *Structure*, **16**, 673–683.
- Velazquez-Muriel, J.A. et al. (2006) Flexible fitting in 3D-EM guided by the structural variability of protein superfamilies. *Structure*, **14**, 1115–1126.
- Volkman, N. and Hanein, D. (1999) Quantitative fitting of atomic models into observed densities derived by electron microscopy. *J. Struct. Biol.*, **125**, 176–184.
- Volkman, N. et al. (2000) Evidence for cleft closure in actomyosin upon ADP release. *Nature Struct. Biol.*, **7**, 1147–1155.
- Wriggers, W. (2004) Spanning the length scales of biomolecular simulation. *Structure*, **12**, 1–2.
- Wriggers, W. and Chacón, P. (2001) Modeling tricks and fitting techniques for multi-resolution structures. *Structure*, **9**, 779–788.
- Wriggers, W. et al. (1998) Self-organizing neural networks bridge the biomolecular resolution gap. *J. Mol. Biol.*, **284**, 1247–1254.
- Wriggers, W. et al. (2000) Domain motions of EF-G bound to the 70S ribosome: insights from a hand-shaking between multi-resolution structures. *Biophys. J.*, **79**, 1670–1678.
- Wriggers, W. et al. (2004) Topology representing neural networks reconcile biomolecular shape, structure, and dynamics. *Neurocomputing*, **56**, 365–379.

# Supplementary Tables

**Table 1.** Evaluation of the interpolation methods.

System	Feature Vectors	Resolution of Map	Rigid Body		Constrained	Splines									IDW					
			Registration		MD	TPS			EBS Kernel 1†			EBS Kernel 2‡			Global‡			Local§		
			RMSD	CC	CC	RMSD	CC	Time	RMSD	CC	Time	RMSD	CC	Time	RMSD	CC	Time	RMSD	CC	Time
RNAP	15	15	6.65	0.86	0.88	3.17	0.88	0.3	3.83	0.87	1.0	3.26	0.88	1.0	1.81	0.88	0.2	1.79	0.88	0.3
GroEL	112	14	6.11	0.96	0.96	4.01	0.93	5.3	3.34	0.96	21.0	3.70	0.97	21.0	2.75	0.95	3.3	2.71	0.95	3.7
Myosin	10	14	5.27	0.91	0.95	2.36	0.94	0.1	1.93	0.94	0.3	2.16	0.94	0.3	1.87	0.94	0.1	1.80	0.95	0.1

Map resolution shown in Å. RMSD measures the  $C_\alpha$  root-mean squared deviation (in Å) between interpolation-based model and constrained MD-based model. CC represents the cross-correlation coefficient to the experimental map. † elasticity coefficient  $\nu = 0.5$ . ‡ weighting power  $c = 8$ . § weighting power  $c = 4$ , and the radius of influence  $R$  encompassing nine feature vectors. Time represents the execution time (in seconds) on an Intel Core 2 duo, 2.4GHz, with 4GB RAM.

**Table 2.** Parameter robustness of IDW and effect of stereochemical idealization.  $C_\alpha$  RMSD in Å.

System	Test 1†	Test 2‡	Test 3§	RefMac*
RNAP	1.81	1.81	1.82	1.66
GroEL	2.82	2.73	2.75	2.49
Myosin	1.82	1.82	1.87	1.71

† Local IDW,  $R$  holding 60% vectors,  $c$  set from 3-4 in 0.2 increments (average RMSD). ‡ Local IDW,  $R$  holding 50-90% vectors in 10% increments,  $c = 3.5$  (average RMSD). § Global IDW,  $c$  set from 7-9 in 0.4 increments (average RMSD). \* Local IDW,  $R$  holding 9 vectors and  $c = 4$ , post-processed with 20 iterations of RefMac (see text). The RMSD values are nearly identical to the values given in Supplementary Table 1.